Food Hydrocolloids 160 (2025) 110820

Contents lists available at ScienceDirect

Food Hydrocolloids

journal homepage: www.elsevier.com/locate/foodhyd

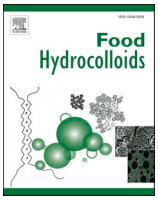

Rubisco at interfaces II: Structural reassembly enhances oil-water interface and emulsion stabilization

Xingfa Ma, Mehdi Habibi, Jasper Landman, Leonard M.C. Sagis, Penghui Shen *

Laboratory of Physics and Physical Chemistry of Foods, Wageningen University, Bornse Weilanden 9, 6708 WG, Wageningen, the Netherlands

ARTICLE INFO

Keywords:
Rubisco
Molecular structure
Oil-water interface
Interfacial rheology
Emulsifying properties
Shear stability

ABSTRACT

Rubisco is the most abundant protein on earth and has gained extensive attentions as a novel food ingredient, such as an emulsifier. Extraction methods can significantly affect its molecular structures and consequently influence its oil-water interface and emulsion stabilization properties. This work aims to elucidate the role of the Rubisco molecular structure in stabilizing the oil-water interface and the multiphase system of emulsions. Ultrafiltration (mild) and acid precipitation-alkaline redispersion (extensive) were used to extract Rubisco from spinach leaves. Protein molecular properties were characterized by size exclusion chromatography (SEC), circular dichroism (CD), and fluorescence spectrometry. Subsequently, the oil-water interfacial properties, including the adsorption and rheological behavior in both small and large dilatational and shear deformations, and the emulsion stabilization properties of Rubisco were investigated. We found that acid precipitation-alkaline redispersion produced a Rubisco extract (RA) with extensive structural reassembling, compared to the one produced by ultrafiltration (RU), for which nativity was mostly retained. RA had two-fold higher surface hydrophobicity than RU, and this caused RA to adsorb faster to the oil-water interface and developed a stiffer solid-like interface ($G_i' = 26 \pm 3$ mN/m) than RU ($G_i' = 15 \pm 2$ mN/m), which was also more resistant to density changes in large dilatational deformations. Consequently, RA displayed higher emulsifying activity and emulsion stability to coalescence during bulk shear and storage. Additionally, structural reassembly resulted in a higher value of the zeta potential of RA, which made the emulsion more stable against flocculation, compared to RU. Our study demonstrates that structural reassembly might be a useful strategy to improve the behavior of plant proteins in oil-water interface and emulsion stabilization, and may stimulate the development of new plant protein-stabilized emulsion-based products.

1. Introduction

Over the past decades, due to the increased need for sustainable and healthy diets, food development has shown a gradual shift from the use of animal-based proteins to plant-based proteins (Aiking & de Boer, 2020; Tziva, Negro, Kalfagianni, & Hekkert, 2020). Rubisco, or ribulose-1,5-bisphosphate carboxylase/oxygenase, the most abundant protein on earth mainly exists in green leaves to fix carbon (Tanambell, Møller, Roman, Corredig, & Dalsgaard, 2023), has gained wide interest in the food industry due to its promising functionalities (e.g. emulsifying properties). Rubisco has been identified as a good emulsifier in many studies (Delahaije, Kiskini, & Wierenga, 2022; Lamsal, Koegel, & Gunasekaran, 2007; Pérez-Vila, Fenelon, O'Mahony, & Gómez-Mascaraque, 2024; Rawiwan & Quek, 2024; Tan, Lee, Martens, & McClements, 2022). Tan et al. (2022) have shown that Rubisco could produce emulsions with a small droplet size ($d < 350$ nm) at a lower concentration than soy and whey protein. Delahaije et al. (2022) found that sugar beet leaf protein had similar emulsifying efficiency, i.e., similar critical concentrations to prevent coalescence and flocculation during emulsification to soy and whey proteins. Despite the good emulsifying properties of Rubisco, the mechanisms by which Rubisco stabilizes the oil-water interface and emulsions are largely unknown.

Rubisco consists of eight large subunits (RbcL) with a molecular weight of 55 kDa each and eight small subunits (RbcS) with a molecular weight of 15 kDa each (Barbeau & Kinsella, 1988; Martin, Castellani, de Jong, Bovetto, & Schmitt, 2019). These two types of subunits combine through hydrophobic interactions and form a globular entity with a final molecular weight of approximately 550 kDa (Xia et al., 2020). Rubisco has been extracted by using extensive or mild extraction methods. Extensive extraction methods, such as alkaline extraction followed by

* Corresponding author.
E-mail address: Bittersweet_Sph@163.com (P. Shen).

https://doi.org/10.1016/j.foodhyd.2024.110820

Available online 5 November 2024

acid precipitation, generally give high protein purities (~90%) (Kobbi et al., 2017), but can also alter the native structure of Rubisco and cause protein denaturation and thus aggregation (Yang & Sagis, 2021). Mild extraction methods, such as ultrafiltration, mostly retain the native structures of proteins. This may affect the functionality of the protein in foam and emulsion stabilization. Indeed, native proteins have been shown to have better air-water interfacial and foaming properties than aggregated protein structures resulting from extensive extraction methods (Geerts, Nikiforidis, van der Goot, & van der Padt, 2017; Kornet et al., 2020).

In part I of this study, we found that Rubisco extracted by ultrafiltration (RU) had better air-water interface and foam stabilization properties than Rubisco extracted by acid precipitation-alkaline redispersion (RA), because RU had a more flexible molecular structure that enabled the formation of stiffer, denser and thicker air-water interfaces, with higher connectivity between proteins, due to the higher level of structure rearrangement and protein-protein in-plane interactions at the air-water interface. However, in terms of emulsifying properties, it appears that extensively extracted proteins may perform better in emulsification than mildly extracted proteins. Denatured soy proteins from extensive extraction methods were found to have better emulsifying properties than the native proteins extracted with mild extraction methods (Palazolo, Sorgentini, & Wagner, 2004), as the denatured proteins have more exposed hydrophobic and hydrophilic regions that can interact more effectively with oil and water phases in the emulsion, respectively (Fan, Liu, Huang, & Li, 2022; Miriani, Corredig, Iametti, & Bonomi, 2011). The air-water interface has an intrinsically different nature from the oil-water interface, for instance, in terms of surface charge (Creux, Lachaise, Graciaa, Beattie, & Djerdjev, 2009) and the difference in polarity between air and oil (El-Mahrab-Robert, Rosilio, Bolzinger, Chaminade, & Grossiord, 2008), which will influence the interfacial behavior of proteins (Sengupta & Damodaran, 1998). To the best of our knowledge, how differences in molecular structure of Rubisco (native or denatured, caused by different extraction methods) influence its oil-water interfacial and emulsifying behavior has not been studied.

In this study, we aim to unravel the mechanisms by which Rubisco stabilizes the oil-water interface and emulsions. Both extensive and mild extraction methods, i.e., acid precipitation-alkaline redispersion and ultrafiltration, were applied to extract Rubisco, producing Rubisco extracts called RA and RU. The molecular properties of RU and RA were characterized by differential scanning calorimetry (DSC), SDS-PAGE, size exclusion chromatography (SEC), dynamic light scatter (DLS), surface hydrophobicity measurement, and circular dichroism (CD). We then systematically investigated the oil-water interfacial properties of RU and RA by measuring the adsorption kinetics and interfacial rheology in both small and large shear and dilatational deformations. Finally, we measured their emulsifying activity and stability against shear and during storage, and linked these macroscopic properties to their molecular and interfacial properties. This study aims to provide a more comprehensive understanding of the relationship between the molecular configuration, interfacial properties and emulsion properties of Rubisco, which may guide the food industry to adjust extraction methods to achieve desired emulsifying properties, not just for Rubisco, but also for other plant proteins.

2. Materials and method

2.1. Materials

Spinach (Spinacia oleracea) and rapeseed oil were purchased from local markets. All chemicals (Sigma-Aldrich, USA) and the materials for SDS-PAGE (Invitrogen Novex, ThermoFisher Scientific, USA) were used as received. Ultrapure water (MilliQ Purelab Ultra, Germany) was used for all experiments unless indicated elsewhere.

2.2. Protein sample preparations

Protein extraction and preparation were the same as in part I of this study (see Sec. 2.2.1-2.2.3). A summary of some important parameters of the extracts is given in Table 1.

2.2.1. Oil stripping

To remove any surface-active impurities, rapeseed oil was purified by mixing with Florisil (100–200 mesh, magnesium silicate, Sigma-Aldrich, USA) at a ratio of 2:1 (v/v) for 16 h at room temperature, followed by centrifuging twice at 2,000g for 20 min to remove residue Florisil. These purified oil samples were stored at −20 °C before further use.

2.2.2. Size exclusion chromatography (SEC)

The protein composition of Rubisco extract was measured by an Akta Pure 25 chromatography system (GE Healthcare, Diegem, Belgium) connected to a UV detector. Initially, 1 wt% of Rubisco extracts were prepared in a 20 mM pH 7.0 phosphate buffer containing 150 mM NaCl and then filtrated over a 0.45 μm syringe filter. Afterward, the filtrated samples were transferred to HPLC vials, and 50 μL of samples were eluted at a flow rate of 0.75 mL/min on a Superdex 200 increase 10/300 GL column (Merck, Schnelldorf, Germany) using the same phosphate buffer as the eluent. The eluted protein were then detected with a UV detector at a wavelength of 214 nm. To identify the molecular weight of the proteins, a calibration curve was measured using aprotin (6.5 kDa), ribonuclease A (13.7 kDa), carbonic anhydrase (29 kDa), ovalbumin (44 kDa), conalbumin (75 kDa), aldolase (158 kDa), ferritin (440 kDa), and dextran (2000 kDa).

2.3. Protein structures

2.3.1. Secondary structure

The protein secondary structure was measured by Far-UV circular dichroism (CD) in a J815 CD spectrometer (JASCO Benelux B.V., NL). Firstly, 0.01 wt% of Rubisco dispersions were prepared in 20 mM pH 7.0 phosphate buffer. The protein dispersions were then injected into a 1.0 mm quartz cuvette, and subsequently measured at wavelength from 190 to 250 nm. Pure phosphate buffer was used as blank, and its intensity was subtracted from the intensity of the protein samples. Lastly, the percentage (%) of each protein secondary structure was calculated using online CD structure prediction software called BeStSel (Ntone, Bitter, & Nikiforidis, 2020).

2.3.2. Tertiary structure

The protein tertiary structure was measured by a fluorescence spectrometer (Shimadzu RF 6000 Fluorometer). Briefly, the protein dispersions were prepared at 0.01 wt% in 20 mM pH 7.0 phosphate buffer. Afterward, 3 mL of protein dispersions were transferred to a disposable cuvette, and then the fluorescence spectrum was measured at an emission wavelength of 285 nm and an excitation wavelength over 300–400 nm.

Table 1
Summary of protein physiochemical properties of Rubisco from part I of this study.

	RA	RU
Peak particle size (nm)	20.5	13.1
Zeta potential (mV)	−20.2 ± 0.9	−14.6 ± 1.2
Surface hydrophobicity (A.U.)	54.9 ± 1.0	15.9 ± 0.7
Denaturation enthalpy (J/g protein)	0.04 ± 0.03	5.19 ± 0.13

2.4. Oil-water interfacial properties of Rubisco

2.4.1. Adsorption behavior

The oil-water adsorption behavior of Rubisco was measured by an automated drop tensiometer (Tecils, France). Briefly, a rising oil droplet with 30 mm^2 area was generated at the tip of a G18 needle in the 0.1 wt % protein dispersion. Subsequently, the oil droplet was equilibrated for 3 h while continuously monitoring the interfacial tension. The droplet shape was analyzed using the built-in software by fitting with the Young-Laplace equation to calculate the interfacial tension. All measurements were performed at least in triplicate at 20 °C.

2.4.2. Interfacial shear rheology

The interfacial shear rheology of Rubisco extracts was measured with a stress-controlled MCR 302e rheometer (Anton Paar, Graz, Austria) fitted with a double-wall ring (DWR) geometry. Briefly, aliquots of 15 mL 0.1 wt% of protein dispersions were pipetted into a Teflon double wall trough, and the DWR was positioned at the liquid interface. Subsequently, aliquots of 7.5 mL of rapeseed oil were pipetted on top of protein dispersions, such that the DWR was located at the oil-water interface. Then, a time sweep was conducted at a strain of 0.1% and frequency of 0.1 Hz within for 3 h. Afterward, frequency sweeps were performed from 0.01 Hz to 2 Hz at a fixed strain of 1%, followed by strain sweeps from 0.01% to 100% at a fixed frequency of 0.1 Hz. The data from frequency sweeps were fitted with a power law equation to obtain the exponent. For the amplitude sweeps, the non-linear rheological behaviors were analyzed using Lissajous plots, which were further quantitatively analyzed by calculating the energy dissipation ratio for each Lissajous plot, according to Ewoldt, Hosoi, and McKinley (2008).

2.4.3. Interfacial dilatational rheology

For the interfacial dilatational rheology, time sweeps were initially conducted during the 3 h of protein adsorption, at an amplitude of 3% and a frequency of 0.02 Hz. After 3 h of stationary adsorption, frequency sweeps were performed at a frequency from 0.005 Hz to 0.01 Hz and a fixed amplitude of 3%. The frequency data were fitted with a power law model ($E_d' \sim \omega^n$, where E_d' is the dilatational storage modulus and ω is the frequency). The amplitude sweeps were conducted at an amplitude from 1% to 60% and at a fixed frequency of 0.02 Hz. Five oscillation cycles were performed in each amplitude and the middle three cycles were used for further data analysis. The rheological data from amplitude sweeps were analyzed by constructing Lissajous plots according to Sagis and Fischer (2014). To further analyze the contributions from network disruption and surface density change during oscillation, these Lissajous plots were analyzed by a general stress decomposition method (GSD) (de Groot, Yang, & Sagis, 2023).

2.5. Emulsifying properties

2.5.1. Emulsion preparation

Before emulsion preparations, protein stock dispersions were prepared at 0.2 wt% and 1 wt% soluble protein concentrations in 20 mM pH 7.0 phosphate buffer and passed through 0.22 μm syringe filters to remove insoluble materials. Coarse emulsions were initially prepared by blending protein dispersions with rapeseed oil at a ratio of 9:1 (w/w) using a high-speed blender (UltraTurrax, IKA, Staufen, Germany) at 12,000 rpm for 2 min. The coarse emulsions were subsequently homogenized using a GEA high-pressure homogenizer (Niro Soavi NS 1001 L, Parma, Italy) for 10 cycles at 180 bars. Lastly, 0.02% NaN_3 was added to the emulsions to prevent the growth of microorganisms. The emulsions were allowed to stand for 24 h to let the interfacial layer be well formed before further analysis.

2.5.2. Zeta potential

The zeta potential of emulsions was measured with a ZetaSizer Nano ZS (Malvern Instruments, UK). The emulsions were initially diluted 200 folds using 20 mM pH 7.0 phosphate buffer. A refractive index of 1.469 and 1.330 was used for rapeseed oil and continuous phase. All measurements were performed in triplicate at 20 °C.

2.5.3. Droplet size distributions

The droplet size distribution of the emulsions was measured by a Mastersizer 3000 (Malvern Panalytical, UK) using a refractive index of 1.469 for rapeseed oil. The emulsions were first measured in water and these measurements were running in triplicate. Subsequently, the emulsions were mixed with 1% SDS solutions at a 1:1 (v/v) ratio to break any clusters of flocculated droplets, and analyzed with the same measurement procedures.

2.5.4. Shear stability

Aliquots of 3 mL of freshly prepared 1 wt% emulsions were subjected to high shear rate treatment using a high-speed blender (UltraTurrax, IKA, Staufen, Germany) at 5000 rpm for 1 min. Afterward, the samples were mixed with 1% SDS solutions and droplet size was measured using the Mastersizer 3000.

2.5.5. Storage stability

Emulsions were stored at 4 °C for two months, and the volume-based mean diameter ($D_{4,3}$) of the emulsions was measured during the storage period. The flocculation (%) and coalescence (%) index of the emulsions were calculated based on the following equations, according to Yang et al. (2024):

$$\text{Flocculation index (\%)} = \frac{D_{4,3} \text{ in water} - D_{4,3} \text{ in SDS}}{D_{4,3} \text{ in SDS}} \quad (1)$$

$$\text{Coalesence index (\%)} = \frac{D_{4,3} \text{ in SDS during storage} - D_{4,3} \text{ in SDS in day 1}}{D_{4,3} \text{ in SDS in day 1}} \quad (2)$$

2.6. Statistical analysis

One-way analysis of variance (ANOVA) was performed with OriginPro 2021. Duncan tests were used for comparison of mean values among determinations using a level of significance of 5%.

3. Results and discussion

3.1. Molecular properties of Rubisco extracts

In part I of this study, we have shown that the mildly extracted Rubisco by ultrafiltration (RU) had a protein content of 78.6%, which was lower than the Rubisco extracted by acid precipitation-alkaline redispersion (RA) (90.7%). The physicochemical properties of RA and RU obtained from part I of the study were summarized in Table 1. Both RU and RA had high protein solubility, which was 95.8% for RU and 91.7% for RA. RU retained most of the nativity of Rubisco, possessing smaller particle size (~13.1 nm), and a low value of the zeta potential (−14.6 ± 1.2 mV), while RA was fully denatured and formed protein aggregates with larger particle size (~20.5 nm), higher value of the zeta potential (−20.2 ± 0.9 mV), and nearly two-fold higher surface hydrophobicity. The molecular structure of RU was mainly stabilized by hydrophobic interactions, and it was more flexible than that of RA, which was primarily stabilized by disulfide bonds.

The protein aggregation states of RU and RA were also evaluated by size exclusion chromatography (SEC) in this study. The SEC chromatogram of RA shows a single narrow peak with a molecular weight of around 1260 kDa (Fig. 1). According to Sanchez de Jimenez, Medrano, and Martinez-Barajas (1995), the native Rubisco multimeric structure has a molecular weight of approximately 550 kDa. Therefore, RA is an aggregate probably consisting of 2–3 Rubisco molecules. As for RU, its

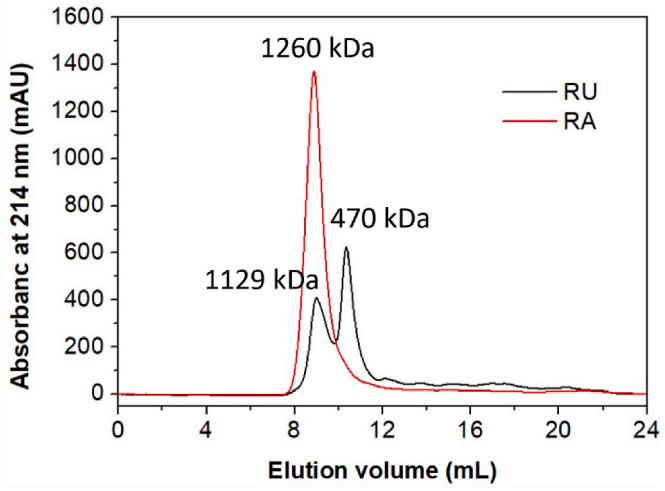

Fig. 1. (A) Size exclusion chromatography (SEC) of Rubisco extracted by ultrafiltration (RU) and acid precipitation-alkaline redispersion (RA) in 20 mM pH 7.0 phosphate buffer containing 150 mM NaCl measured at the wavelength of 214 nm.

molecular weight has a bimodal distribution in SEC (Fig. 1) with a major peak at around 470 kDa and a minor peak at around 1130 kDa, which corresponds to native Rubisco and Rubisco aggregates, respectively. The results from SEC agree with the SDS-PAGE results from part I of this study, where RA mainly consisted of aggregates in nonreducing conditions, while RU mostly showed the two subunit bands of Rubisco.

We further determined the secondary and tertiary structures of RU and RA. RA has a lower α-helix content (15.1 ± 1.1%) than RU (22.4 ± 0.3%) (p = 0.011) (Fig. 2A), and it has slightly higher β-sheet and random coil contents. The decrease of α-helix content in RA might be caused by the pH-shifting processing, which was reported to disrupt the hydrogen bonds between the first carbonyl oxygen (–CO) and the fourth amino hydrogen (–NH) in the α-helix structures (Cabra, Arreguin, Vazquez-Duhalt, & Farres, 2006; Dumetz, Chockla, Kaler, & Lenhoff, 2008; Skipper et al., 1996). Regarding the tertiary structure, the fluorescence emission of RA shows a slight red shift by 2.5 nm and reduced maximum fluorescence intensity by 14.0 % (Fig. 2B), which could be ascribed to the exposure of Tryptophan residues to the polar water environment that caused fluorescence quenching of Tryptophan by water molecules.

Overall, the extensively extracted Rubisco RA has pronounced molecular structural reassembling in the secondary, tertiary and quaternary levels compared to mildly extracted Rubisco RU, leading to a higher amount of surface ionic groups and increased surface hydrophobicity.

3.2. Adsorption behavior of Rubisco at oil-water interface

The oil-water adsorption behavior of RA and RU was measured with a drop tensiometer. After 1 s of adsorption, RA already shows a higher interfacial pressure than RU, implying that RA might have a shorter adsorption induction time and thus adsorbs faster to the interface than RU (Fig. 3A). The main particle size of RU is nearly one-fold smaller than that of RA, and smaller protein molecules are expected to diffuse faster than large ones as shown in part I of this study where RU adsorbed faster to the air-water interface than RA. However, the higher surface hydrophobicity of RA gives it a higher affinity for the oil-water interface, and that promotes the adsorption (Wierenga, Meinders, Egmond, Voragen, & de Jongh, 2003). After this initial phase, the surface pressure increases faster for RU than RA and finally reaches a value of 16.1 ± 0.2 mN/m, slightly higher than RA (15.6 ± 0.3 mN/m). The evolution of the surface pressure with time of both RA and RU follows logarithmic aging behavior between 100 s and 3 h (Fig. S1) (R^2 = 0.98 and 0.99 for RA and RU, respectively), which is a common feature for disordered solid-like systems (Shohat, Friedman, & Lahini, 2023).

To monitor the time evolution of the mechanical properties of the oil-water interface during protein adsorption, the oil-water interfaces were also subjected to oscillatory interfacial shear deformations at a strain of 0.1% and frequency of 0.1 Hz. The storage moduli (G_i') of RA and RU are already higher than their loss moduli (G_i'') after 60 s of adsorption, indicating the fast development of viscoelastic solid-like oil-water interfaces by both RA and RU, similar to their behavior at air-water interfaces in part I of this study. Within 3 h of measurement, the G_i' of RA is always higher than that of RU, indicating that the RA-stabilized interface is stiffer than the RU-stabilized interface, likely ascribed to the higher surface hydrophobicity of RA (Table 1), which might increase the protein-protein in-plane interactions through hydrophobic interactions. Interestingly, the time evolution of the moduli G_i' of both RA and RU follow power law behavior during the whole 3 h of adsorption. Their exponents from the power law fitting are comparable to each other with a value around 0.3 (Table S1). As to the time sweep from dilatational rheology, both RA and RU form a comparably stiff oil-water interface during 3 h of adsorption, where the RA-stabilized interface followed power-law behavior during the whole adsorption time range with exponent of 0.08, and the RU-stabilized interface started to follow power-law behavior after 1000 s of adsorption, with an exponent of 0.05 (Fig. S2). The G_i' and E_d' of the interfaces formed by RA and RU also followed power-law behavior with adsorption time at air-water interfaces, indicating the similar nature of these interfaces to structural glass-like disordered materials (Negi & Osuji, 2010). Also, RA- and RU-stabilized interfaces have similar aging behavior in the increase in stiffness at the oil-water interface; while at the air-water interface, the RA-stabilized interface showed a pronouncedly slower growth of stiffness, exhibiting that these two types of interfaces can have a different impact on the interfacial aging behavior of proteins.

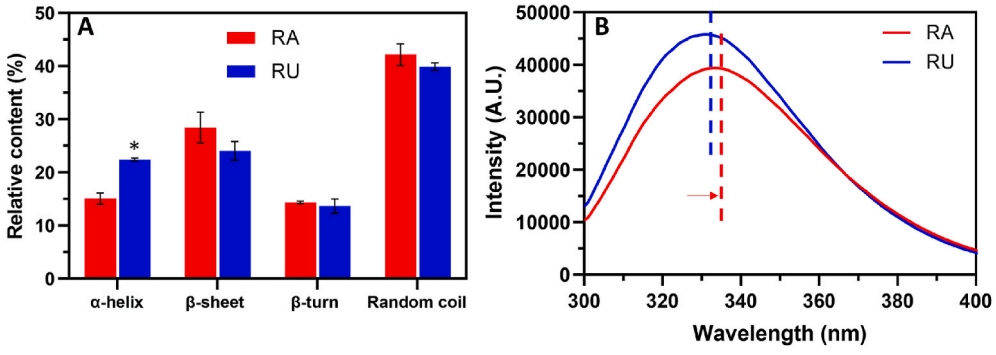

Fig. 2. Secondary structure content (A), and intrinsic fluorescence intensity (B) of 0.1 wt% RA and RU in 20 mM pH 7.0 phosphate buffer.

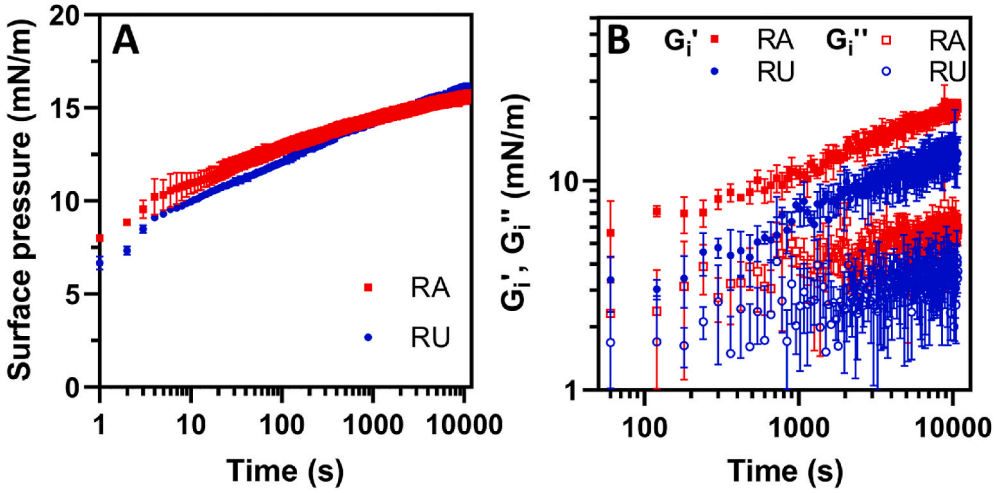

Fig. 3. (A) Interfacial pressure (mN/m) as a function of time (s) of RA and RU. Protein dispersions were prepared at 0.1 wt% protein concentration in 20 mM phosphate buffer. (B) The interfacial shear storage modulus (G_i') and loss modulus (G_i'') of RA and RU as a function of time (s).

3.3. Oil-water interfacial rheological behavior of Rubisco

3.3.1. Interfacial shear rheology

After 3 h of adsorption, the oil-water interfaces stabilized by RA and RU were further subjected to frequency sweeps (0.01–2 Hz at a fixed strain of 1%). Both interfaces show weak frequency dependency (Fig. 4A), which generates *n* values lower than 0.2 (obtained from power-law fitting, $G_i' \sim \omega^n$) (Fig. 4B), similar to air-water interfaces stabilized by RA and RU in part I of this study. These low *n* values indicate that the structures formed by RU and RA at the interface have a wide spectrum of relaxation times in shear, which is typical for disordered soft glasses and chemical gels (Winter & Mours, 1999).

In the strain sweeps (0.1–100% at a fixed frequency of 0.1 Hz), both interfaces stabilized by RA and RU show independence of G_i' on strain in the low strain regime, which represents the linear viscoelastic regime (LVE). The length of LVE is comparable for RA (2.6 ± 0.5%) and RU (2.3 ± 0.8%). In the LVE regime, RA has a higher G_i' (25.7 ± 2.6 mN/m) than RU (14.7 ± 2.5 mN/m) as also observed in both time sweeps and frequency sweeps. When the strain increases, the moduli G_i' of both interfaces start to decrease with strain due to the disruption of interfacial network structures, and the response of the interfaces enters the nonlinear viscoelastic (NLVE) regime. But the values for G_i' stay higher than those for G_i'' for the entire applied strain range. The Gi' of RA is higher than that of RU also in the NLVE regime, indicating that the RA-stabilized interface is still stiffer than the RU-stabilized interface under large shear deformations. At the air-water interface, both RA and RU have a higher G_i' (39–56 mN/m) especially for RU (56.0 mN/m), but a shorter length of the LVE (1.4–1.6%). The considerable decrease of Gi' and the increased LVE range of RA- and RU-stabilized oil-water interfaces suggest that these interfaces have weaker protein-protein in-plane interactions but higher stretchability.

In the calculation of these moduli, only the first harmonic of the Fourier transform spectrum is involved, but in the NLVE regime, higher-order harmonics are present in the stress responses, which can be further analyzed using Lissajous plots. The Lissajous plots of RA and RU at 0.5% strain (in the LVE regime) show narrow elliptical shapes (Fig. 5B), implying linear viscoelastic behavior dominated by elastic components. When the strain enters the NLVE regime, all plots become wider, indicating an increased viscous contribution to the total stress response due to the disruption of the interfacial network structure. When the strain increases to 100%, all plots show a gradual transition to plastic behavior with a positive slope of the elastic component at the origin, indicating that the interfacial network structures of RA and RU were severely disrupted in the large shear deformation but still retained pronounced elastic components. At the extremes of the intracycle deformation, the Lissajous plots of both RA and RU display strain hardening (the slope of the elastic component increases), which is due to the stretching of the residual interfacial network structure.

To further quantitatively analyze the interfacial structure disruption with the Lissajous plots, the energy dissipation ratio (Φ) was calculated

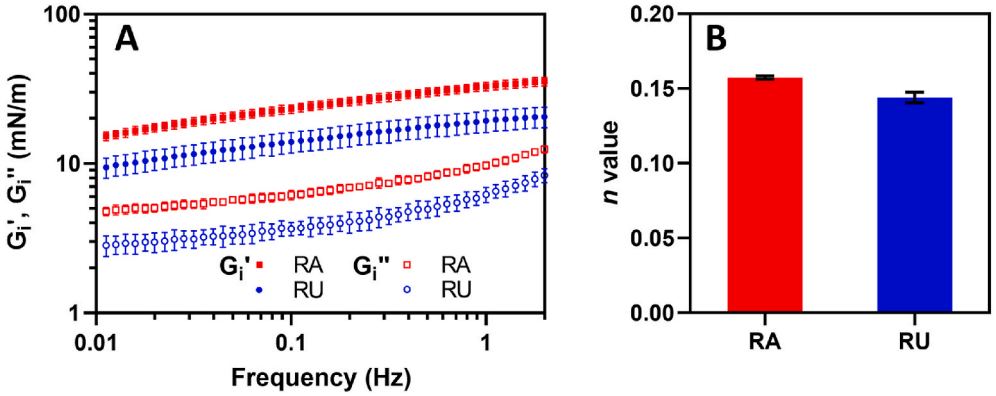

Fig. 4. (A) The surface shear storage modulus (G_i') and loss modulus (G_i'') of RA and RU as a function of frequency (Hz). (B) The values of exponent n obtained from the power-law fitting $G_i' \sim \omega^n$ of the interfacial shear frequency sweeps at a fixed strain of 1% for RA and RU. Both dispersions were prepared at 0.1 wt% protein concentration in 20 mM phosphate buffer.

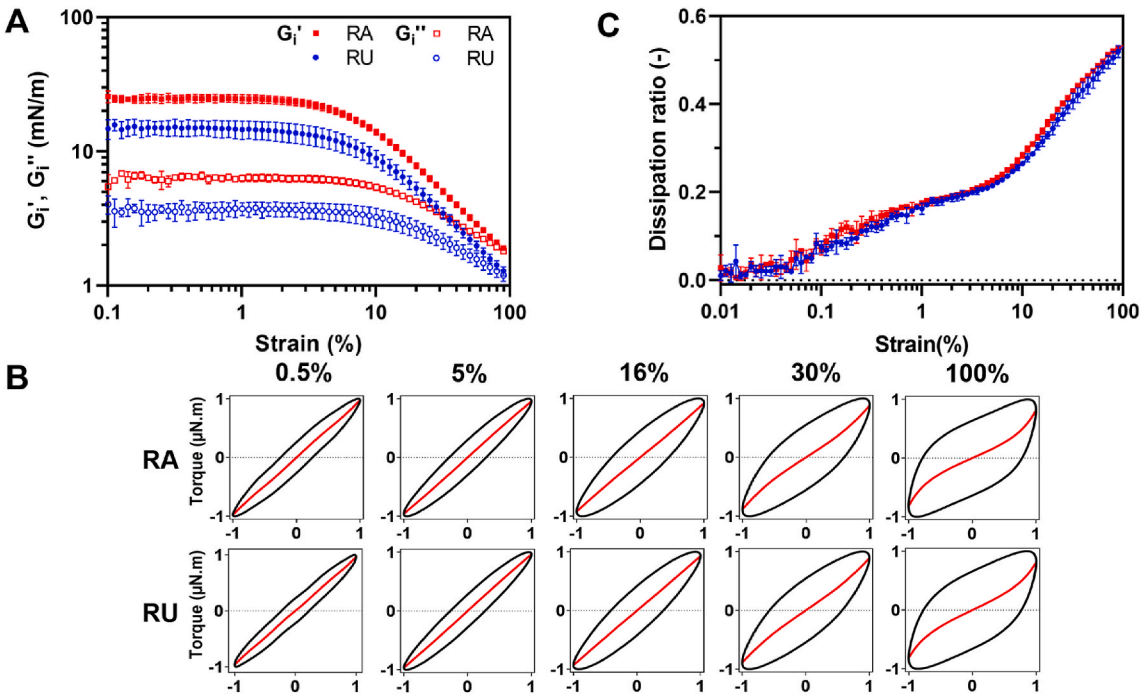

Fig. 5. (A) The surface shear storage modulus (G_i') and loss modulus (G_i'') of RA and RU as a function of strain (0.1–100 %) and a fixed frequency of 0.1 Hz for RA and RU. (B) Normalized Lissajous plots (black circle) and the decomposed elastic components (red lines) at 0.5%, 5%, 16%, 30%, and 100% and a fixed frequency of 0.1 Hz for RA and RU. (C) The dissipation ratio of RA and RU with the increased strain (%) from 0.01% to 100%. Both dispersions were prepared at 0.1 wt% protein concentration in 20 mM phosphate buffer.

based on the area enclosed by Lissajous plots, according to the method proposed by Ewoldt et al. (2008). In the whole strain range (0.1–100%), RA and RU show comparable Φ values, indicating their similar linear and nonlinear rheological behavior in response to small and large shear deformations at oil-water interfaces, which also happened at air-water interfaces in the part I of this study. In the LVE regimes, the Φ values of all interfaces were smaller than 0.2, suggesting a predominant elastic behavior of the interfaces. In the NLVE regimes, the Φ values of RA and RU exhibit substantial increases to around 0.53 at 100% strain, indicating extensive interfacial structure disruption. But those Φ values are pronouncedly lower than 1 which indicates purely plastic behavior and complete structure disruption, suggesting a partial retainment of the interfacial network structure.

3.3.2. *Interfacial dilatational rheology*

The oil-water interfacial mechanical properties of RA and RU were also investigated by applying dilatational rheology (Fig. 6). After 3 h of adsorption, the interfaces were subjected to frequency sweeps or amplitude sweeps. In the frequency sweeps (0.005–0.1 Hz at a fixed strain of 3%), similar to those performed in shear deformation, the interfaces stabilized by both RA and RU show weak frequency dependency (Fig. 6A). The n values calculated from power-law fitting ($E_d' = \omega^n$) are much lower than 0.5, which indicates that in the LVE regime there is limited exchange of material between interface and bulk (Lucassen & Van Den Tempel, 1972) (Fig. 6B), suggesting that in-plane protein interactions or momentum transfer between bulk and interface play a main role in the dilatational stress response. Those low n values confirm that RA- and RU-stabilized interfaces have disordered solid-like characteristics (Moghimikheirabadi, Fischer, Kröger, & Sagis, 2019).

In the amplitude sweeps (1–60% deformation amplitude at a fixed frequency of 0.02 Hz) (Fig. 6C), RA and RU show comparable E_d' in the whole range of deformation amplitudes, suggesting the high similarity in their interfacial behavior in dilatational deformation. The interfaces display a linear viscoelastic regime (LVE) at small deformation amplitudes up to 3–4% and with an E_d' around 32 mN/m. After that, the E_d' starts to visibly decrease due to the disruption of interfacial structure or the pronounced change of interfacial density. The E_d' of both RA and RU are always higher than the E_d'', suggesting that RA- and RU-stabilized interfaces are still solid-like at large dilatational deformations. Finally, the E_d' of RA and RU decreased to ~14.5 mN/m at 60% deformation amplitude. The moduli E_d' of RA- and RU-stabilized oil-water interfaces at a deformation amplitude of 1% are much lower than those of the air-

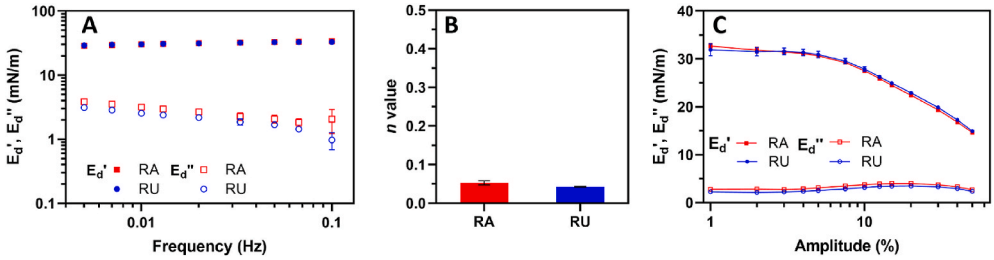

Fig. 6. Interfacial dilatational storage modulus (E_d') and loss modulus (E_d'') as a function of frequency (Hz) (A) and deformation amplitude (%) (C). (B) The value of exponent n obtained from the power-law fitting $E_d' \sim \omega^n$ of the interfacial dilatational frequency sweeps at a fixed amplitude of 3% for RA and RU. Both dispersions were prepared at 0.1 wt% protein concentration in 20 mM phosphate buffer.

water interfaces (84–98 mN/m), confirming that RA and RU have considerably weaker in-plane interactions at the oil-water interface.

To analyze the contributions of the higher-order harmonics in the non-linear behavior of RA and RU at the oil-water interface at large dilatational deformation, Lissajous plots were constructed and analyzed. At 5% deformation amplitude, the Lissajous plots of RA and RU are nearly closed lines, indicating linear and almost purely elastic responses (Fig. 7). At higher deformation amplitudes (10–50%), the plots become wider and more asymmetric due to interfacial structure disruption and/or density changes, and a tail appears at the left corner of the plots due to interface buckling caused by interfacial jamming, especially for those at 40% and 50% deformation amplitudes (Fig. 7). Such nonlinear behavior did not occur at the air-water interface at the same large deformations. To further analyze these nonlinearities in Lissajous plots and distinguish the contributions from interfacial structure disruption and density changes, we used the general stress decomposition (GSD) method (de Groot et al., 2023) to decompose the Lissajous plots in the next section.

3.3.3. General stress decomposition

In the general stress decomposition (GSD), the total stress is split into two contributions, one consisting of all odd and one containing all even harmonics. The former describes the nonlinearities which correspond to interfacial network disruption, and the latter quantifies nonlinearities resulting from surface density changes. The odd harmonics can be split further in an elastic (τ_1) and viscous (τ_2) stress component, while the even harmonics also include contributions quantifying energy storage (τ_4) and dissipation (τ_3). Here, τ_1 and τ_4 are curves, τ_2 and τ_3 are loops. We only decomposed the Lissajous plots at 1–30% strains, since those from 40 to 50% strains have visible tails due to interfacial buckling, and when this phenomenon occurs, density changes also produce contributions to the odd harmonics. The GSD can then no longer separate contributions stemming from network disruptions and density changes.

We plotted the decomposed Lissajous plots and their combinations at 20% strain as an example in Fig. 8. The odd harmonics in Fig. 8B and F shows a narrow and nearly linear ellipsoidal shape, implying that the elastic component dominates the stress related to interfacial network changes. RA shows an overall comparable slope of τ_1 as RU, indicating the comparable stiffness of the interfaces stabilized by these proteins. The τ_4 curve of the RA-stabilized interface shows a more negative value at the extremes of intracycle deformation than the RU-stabilized interface, suggesting that the RA-stabilized interface has more pronounced contributions from the interfacial density change upon dilatational deformation. Those decomposed stress plots were further subjected to quantitative analysis for a clearer comparison between the nonlinear behavior of RA and RU at the oil-water interface in dilatational deformations. Five parameters were determined including $E_{\tau 1L}$, $U_{\tau 2}$, $U_{\tau 3}$, $E_{\tau 4}$, and γ_s. $E_{\tau 1L}$ and $E_{\tau 4}$ are two secant elastic moduli, describing the interfacial network stiffness and resistance to interfacial density change, respectively. $U_{\tau 2}$ and $U_{\tau 3}$ are two dissipated energies per unit area, from interfacial structure disruption and interfacial density change, respectively. Furthermore, γ_s measures the baseline shift of the oscillation with respect to the initial quasi-equilibrium state and is a measure of how far the oscillations drive the interface out of equilibrium.

The moduli $E_{\tau 1}$ of all interfaces show decreasing trends with increased deformation (Fig. 9A), indicating the disruption of the interfacial network structure. RA shows a slightly higher $E_{\tau 1}$ modulus than RU at the deformation amplitude of 1–2% ($p = 0.02$ at 1% and $p = 0.01$ at 2%), implying that RA-stabilized interface tends to be slightly stiffer than the RU-stabilized interface at small deformations. At larger deformation amplitudes, RA and RU show comparable $E_{\tau 1}$ moduli, which indicates comparable stiffness for these interfaces. The dissipated energy of τ_2 ($U_{d\tau 2}$) of RA tends to be higher than RU (Fig. 8D), suggesting that the RA-stabilized interface initially has stiffer network structures than the RU-stabilized interface and requires more energy to disrupt the interface.

The modulus of τ_4 ($E_{\tau 4}$) of the RA-stabilized interface has a more negative value than that of the RU-stabilized interface, indicating that RA may form a more densely packed oil-water interface and thus be more resistant to surface density changes during large dilatational deformation. This is consistent with its more negative vertical shift of τ_4 (γ_s) (Fig. 9C), since a denser interface would reduce the in-plane mobility of proteins and result in slower relaxation at the interface. As a result, the RA-stabilized interface cannot quickly restore to the quasi-equilibrium state at zero deformation, which therefore causes a more negative shift of τ_4. The possibly denser interface formed by RA could also explain its higher interfacial modulus in shear deformations than the RU-stabilized interface (Fig. 5A and B), as denser interfaces also tend to be more resistant to shear deformation (Tamm & Drusch, 2017). The dissipated energy of τ_3 ($U_{d\tau 3}$) of both RA- and RU-stabilized interface exhibit low values (less than 0.1 mJ/m^2) (Fig. 9E), implying the limited diffusional exchange between bulk and interface even in large dilatational deformation. Compared to the oil-water interface, RA and RU formed a much stiffer network structure at the air-water interface, and they had much more pronounced nonlinear behavior in terms of the value of $U_{\tau 2}$, $U_{\tau 3}$, $E_{\tau 4}$, and γ_s.at large deformations, implying that the oil phase largely depresses the interfacial network stiffness and the nonlinear behavior of proteins.

Overall, RA tends to adsorb faster to the oil-water interface than RU, and the RA-stabilized interface is more resistant to deformation, especially to shear, compared to the RU-stabilized interface. These phenomena are ascribed to the pronouncedly higher surface hydrophobicity of RA than RU, which is expected to increase the affinity of proteins to the oil-water interface and promote the formation of a dense oil-water interface with increased in-plane interactions through hydrophobic

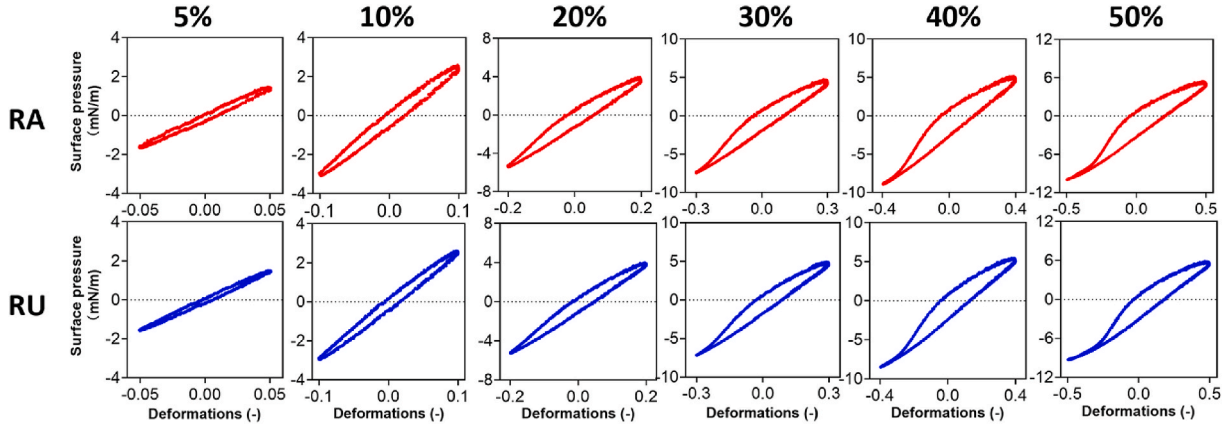

Fig. 7. Lissajous plots of surface pressure as a function of deformation amplitude (5%–50%) for RA and RU. Both dispersions were prepared at 0.1 wt% protein concentration in 20 mM phosphate buffer.

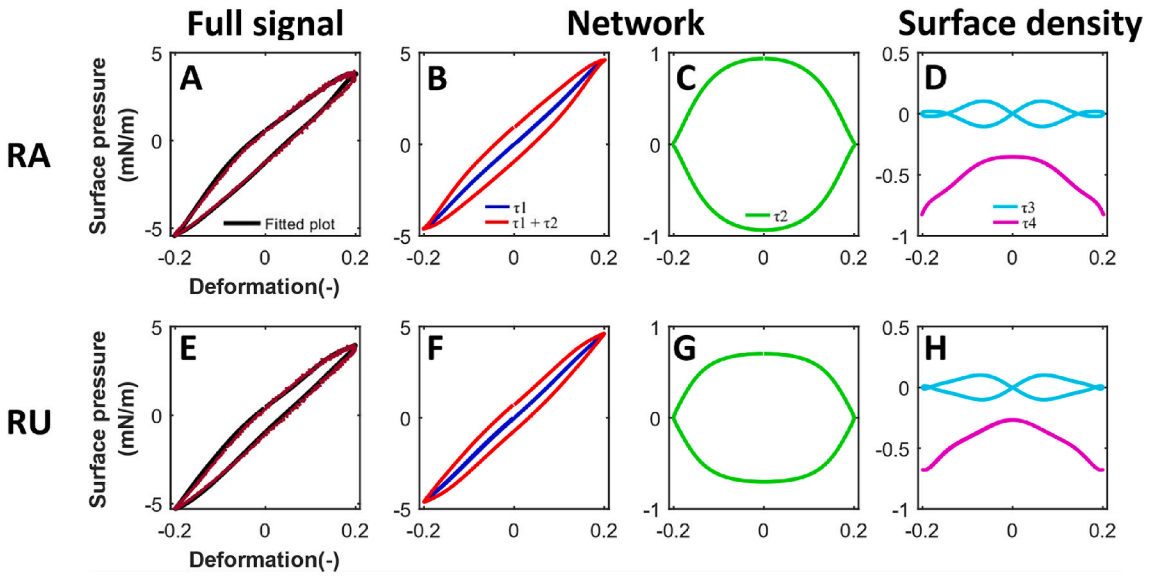

Fig. 8. Decomposed Lissajous plots of RU and RA at a deformation amplitude of 20%. The fitted full signal is shown in black (—), τ_1 is shown in dark blue (—), $\tau_1 + \tau_2$ is shown in red (—), τ_2 is shown in green (—), τ_3 is shown in cyan (—), and τ_4 is shown in magenta (—).

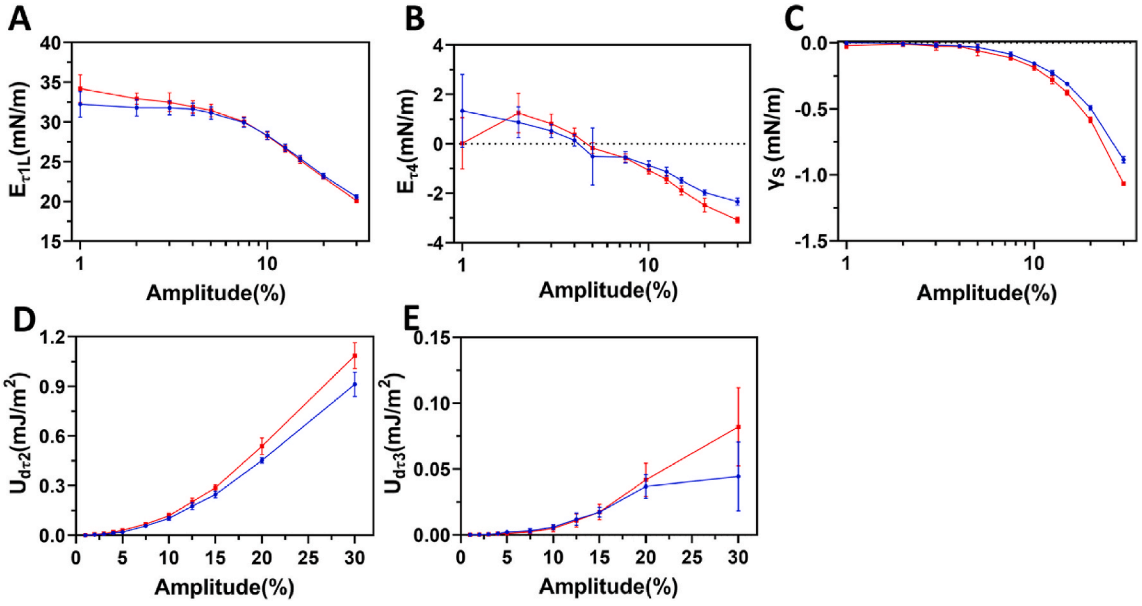

Fig. 9. $E_{\tau 1L}$ (A), $E_{\tau 4}$ (B), γ_s (C), $U_{d\tau 2}$ (D), and $U_{d\tau 3}$ (E) as a function of deformation amplitude (%) for the oil-water interfaces stabilized by RU (in blue) and RA (in red).

interactions. In comparison to the air-water interfacial properties of RA and RU in part I of this study, the native Rubisco sample RU adsorbed faster to the air-water interface than the denatured Rubisco sample RA, due to its smaller particle size and higher conformational flexibility. The RU-stabilized air-water interface had a faster growth of stiffness and higher stiffness after 3 h of adsorption. But these advantages of protein nativity appear to be less important at the oil-water interface, where the higher surface hydrophobicity of RA is a more important factor and enabled a faster increase of interfacial pressure in the early adsorption stages. In interfacial rheology, RU and RA behaved more similarly and the extent of nonlinearity in the response at large strains was lower than at the air-water interface. The oil phase appears to have largely decreased the in-plane interactions between RA or RU, especially for RU, compared to the air-water interface.

These striking differences in the interfacial behavior of RA and RU at the oil-water and air-water interface are highly related to the different nature of the oil and air phase. The air phase has a much lower density and has rather weak interactions with proteins at the air-water interface. As a result, the parts of the proteins protruding into the air phase predominantly interact with each other and tend to generate a stiff network structure. The air phase also has weak interactions with water molecules at the interface, and this causes high surface tension, which would generate high elongation stresses on the proteins and promote protein structural rearrangement or unfolding, which could in turn also promote stronger in-plane interactions (Bergfreund, Diener, et al., 2021). By contrast, the oil phase has a much higher density, and the oil molecules near the interface could interact with the hydrophobic patches at the surface of protein molecules, which would decrease the in-plane hydrophobic interactions between proteins and decrease the interfacial stiffness (Bergfreund, Bertsch, & Fischer, 2021a). The oil molecules

could also interact more with water molecules at the interface through van der Waals interactions/hydrogen bonding and thus lower the interfacial tension, and act as plasticizers, weakening the interfacial network formed by the proteins (Bergfreund, Bertsch, & Fischer, 2021b). Thus, proteins at the oil-water interface tend to behave more like particles with less unfolding and weaker in-plane interactions compared to the air-water interface (Bergfreund, Diener, et al., 2021). This well explained the much lower interfacial stiffness of RU and RA at oil-water interfaces, and that the buckling phenomena only happened at oil-water interfaces for RU and RA when the interfaces were compressed. RA has a nearly two-fold higher surface hydrophobicity than RU, and this could have resulted in somewhat stronger in-plane interactions, and consequently RA formed a stiffer oil-water interface than RU.

3.4. Emulsifying properties

Oil-in-water emulsions were prepared with RA and RU at protein concentrations of 0.2 wt% and 1 wt%. During emulsification, proteins adsorb to the newly formed oil-water interfaces driven by both diffusion and convection, and then form a layer at the interface that prevents the recoalescence of the newly generated oil droplets (McClements, 2004; Perrier-Cornet, Marie, & Gervais, 2005; Walstra, 1993). Several mechanisms are involved in emulsion stabilization by proteins: (1) *charge-based stabilization*: a high protein charge results in strong electrostatic repulsion between oil droplets and thus prevents flocculation and coalescence of the newly formed oil droplets (Mohan & Narsimhan, 1997; Tcholakova, Denkov, Ivanov, & Campbell, 2006); (2) *steric stabilization*: a thick protein layer can provide more steric repulsion between oil droplets and reduce flocculation of emulsion droplets (Malmsten, 1998); (3) *mechanical stabilization*: a stiff protein-stabilized oil-water interface can prevent film rupture between flocculated oil droplets (Amine, Dreher, Helgason, & Tadros, 2014; Wang, Li, Wang, Hao, & Gong, 2014). It should be noted that these factors may work in combination to affect the emulsion stability during post-processing and long-term storage.

3.4.1. Droplet size distributions of fresh emulsions

In Fig. 10A, the fresh emulsions stabilized by 0.2 wt% RA and RU display bimodal distributions, in which the second peak of the RU-stabilized emulsion is at a larger size (10.5 μm) than the RA-stabilized emulsion (6.3 μm). To further investigate the droplet aggregation mechanisms, 1 wt% SDS was added to the emulsions. SDS can cause high electrostatic repulsion forces at the droplet surface and thus diminish the flocculation of oil droplets, to enable the measurement of the single droplet size (Dickinson, 2019). In a 1 wt% SDS solution, the bimodal distributions of those emulsions were reduced to monomodal distributions with peaks at 2.0 μm for both RA- and RU-stabilized emulsions. The surface-weighted mean droplet size ($D_{3,2}$) of RA- and RU-stabilized emulsions were reduced from 3.93 (±0.19) μm and 4.94 (±0.22) μm to 1.35 (±0.03) μm and 1.46 (±0.03) μm, respectively (Fig. 10B). This indicates that a significant degree of flocculation occurred in those emulsions, and the flocculation index of RU-stabilized emulsion is 432 (±55) %, which is much higher than for the RA-stabilized emulsion (272 ± 31%) (Fig. 12C), consistent with light microscopy observations (Figs. S3A and B). The single droplet size of the RA-stabilized emulsion (1.35 ± 0.03 μm) is slightly smaller than that of the RU-stabilized emulsion (1.46 ± 0.03 μm) ($p = 0.014$) although RA has an almost one-fold larger size than RU (Fig. 2A). This phenomenon agrees with the tendency that RA adsorbs faster to the oil-water interface than RU (Fig. 3). With protein concentration increased to 1 wt%, the RA-stabilized emulsion shows a monomodal droplet size distribution with a peak at 1.4 μm, while the RU-stabilized emulsion still shows a bimodal droplet size distribution with a major peak at 4.3 μm. In the 1 wt% SDS solution, the droplet size distribution of the RA-stabilized emulsion only slightly shifts to a smaller droplet size, with the peak at 0.80 μm and $D_{3,2}$ of 0.76 (±0.01) μm. The bimodal distribution of the RU-stabilized emulsion was reduced to a monomodal distribution with a peak at 0.8 nm and $D_{3,2}$ of 0.76 (±0.02) μm. These results suggest that RA-stabilized emulsions are more stable to flocculation than RU-stabilized emulsions, and RA tends to stabilize smaller oil droplets. The lower degree of flocculation in RA-stabilized emulsions could be related to its higher value of the zeta potential (Fig. 10E) induced by the higher value of the zeta potential of RA (Fig. 2B), which could provide

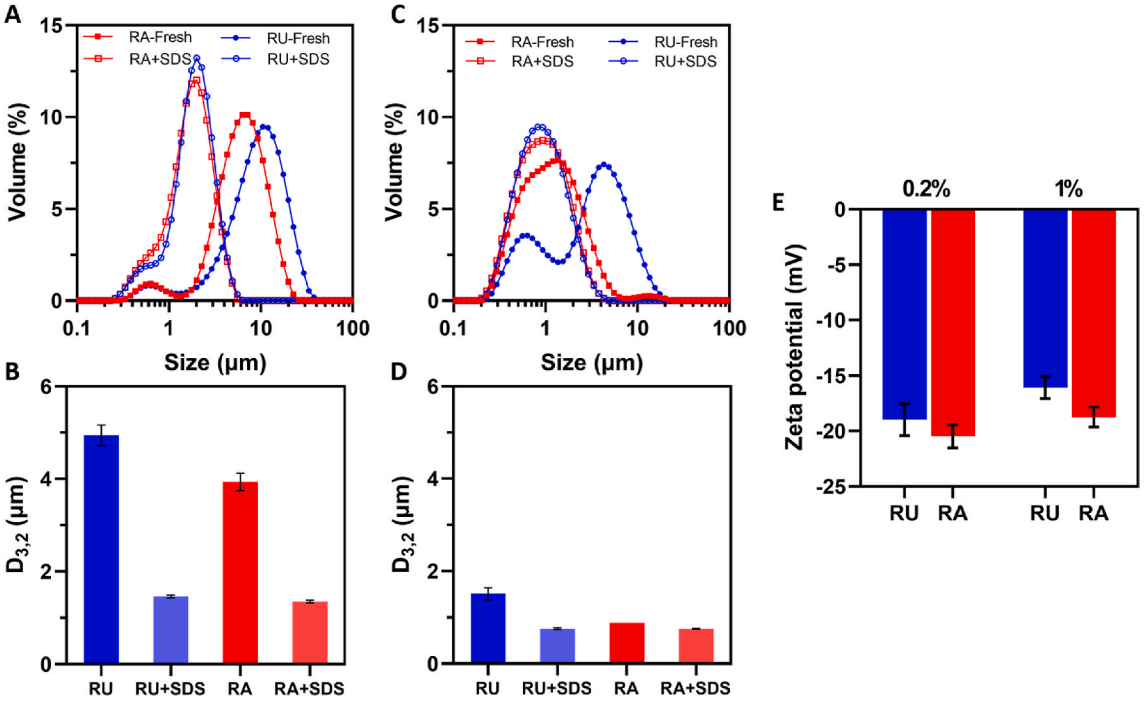

Fig. 10. Droplet size distributions (A and C) and surface-mean droplet size ($d_{3,2}$) (B and D) of freshly prepared emulsions measured in water or in 1 wt% SDS solution for RU and RA at 0.2 wt% (A–B) and 1 wt% protein concentration (C–D). (E) Zeta potential (mV) of those freshly prepared emulsions.

stronger electrostatic repulsions between oil droplets.

3.4.2. Shear stability of fresh emulsions

The emulsions prepared at 1 wt% protein, were subjected to turbulent shear flow (with a shear rate around 500/s near the homogenizing probe) to test their stability in large deformations, which are frequently encountered by emulsions during industrial processing, transportation, and consumption. In this treatment, the surface of the oil droplets will be sheared and deformed, where both large shear and dilatational deformations are involved (Ikenaga & Sagis, 2024). As shown in Fig. 11, after shear processing, the RU-stabilized emulsion clearly displays a minor peak with increased droplet size (Fig. 11D), indicating the coalescence of oil droplets. The occurrence of new peaks is less visible in the RA-stabilized emulsion, and it has less change in the volume distribution (i.e., the of area of new peaks) of droplet size (7.6 ± 0.9 %) than the RU-stabilized emulsion (2.7 ± 0.2 %), although the new peaks seem to span a larger range of droplet sizes. These results suggest that the RA-stabilized emulsion is overall more stable to shear-induced droplet coalescence than the RU-stabilized emulsion, which aligns well with the higher resistance of the RA-stabilized oil-water interface to both large shear and dilatational deformations in the interfacial shear and dilatational rheological measurements (Figs. 5 and 9).

3.4.3. Storage stability of emulsions

The volume-weighted mean droplet size ($D_{4,3}$) of RA- and RU-stabilized emulsions was monitored during two months of storage, and used to calculate the flocculation and coalescence indices of the emulsions, since it is more sensitive to droplet size changes than the surface-weighted mean droplet size $D_{3,2}$.

On day 7, RU-stabilized emulsions at both low and high protein concentrations already formed distinct creaming layers, while these only occurred for RA-stabilized emulsions on day 60 (Fig. 12E). The high creaming stability of RA-stabilized emulsions is because of their initial relatively low flocculation degree compared to the RU-stabilized emulsions, which retards the creaming of the emulsion. At the 0.2 wt% protein concentration, the RU-stabilized emulsion shows decreased flocculation indices (FI) and increased coalescence indices (CI) during the first two weeks of storage, while the RA-stabilized emulsion shows stable FI and keeps a low CI. These phenomena indicate that the RA-stabilized emulsion at the low protein concentration has higher coalescence stability during that storage period, which is ascribed to the higher resistance of the RA-stabilized interface to deformation (Fig. 9). Additionally, RA seemingly can form a more densely packed oil-water interface, indicated by its higher resistance to interfacial density changes than RU (Fig. 9). RA might also form a thicker oil-water interface than RU, in view of its larger particle size (Fig. 2A) and more rigid molecular structure (Fig. 1), and this can also contribute to its higher coalescence stability. On day 60, the RA-stabilized emulsion at the 0.2 wt% protein concentration also showed pronounced coalescence, as indicated by its significantly increased CI (Fig. 12D). At the 1 wt% protein concentration, both RA- and RU-stabilized emulsions showed relatively low CI values (lower than 20%) till the 60th day of storage, indicating that these emulsions were stable against coalescence during long-term storage, probably because of the sufficient surface coverage by proteins compared to those prepared at the 0.2 wt% protein concentration.

Overall, RA tends to have higher emulsifying activity, flocculation stability, and coalescence stability than RU, especially at a relatively low protein concentration.

When comparing part I and part II of this study, we clearly see different effects of the structural changes of rubisco proteins on their behavior at the air-water and oil-water interface. In part I, that studied the air-water interface and foam, rubisco proteins (RU) with a native and flexible molecular structure showed better performance in the interfacial adsorption and the stabilization of the air-water interface and foam than the counterpart (RA), with a denatured and more rigid structure. Nevertheless, the high surface hydrophobicity of RA generated high interfacial stiffness and largely contributed to its good foaming properties. In this part, which studied the oil-water interface and emulsions, RU and RA behaved more like particles with less unfolding and weaker in-plane interactions due to the plasticization effect of oil phase and the interactions with oil molecules at the interface. While the higher surface hydrophobicity and surface charge of RA caused by structural reassembly resulted in better performance in stabilizing the oil-water interface and emulsions compared to RU. The whole study clearly shows that different protein extraction processes could generate protein extracts with largely different molecular structures, which could pronouncedly influence their interfacial behavior and functionalities. High interfacial stiffness and resistance to deformation, and high interfacial charge are important to the stability of foam and emulsions, which could be realized by improving the conformation flexibility, surface hydrophobicity and surface charge of protein molecules.

4. Conclusions

In part II of the whole study, we systematically investigated the effect of the molecular structure of Rubisco, altered by the extraction methods, on its oil-water interfacial and emulsifying properties. The Rubisco extracted by ultrafiltration (RU) retained most of its nativity and mainly consisted of single Rubisco molecules, stabilized primarily by hydrophobic interactions. The Rubisco extracted by acid precipitation-alkaline extraction (RA) showed extensive structural reassembly, and formed aggregates involving 2–3 Rubisco molecules, mainly through disulfide bonds, and had increased surface hydrophobicity and surface ionic groups. The higher surface hydrophobicity of RA resulted in faster adsorption at the oil-water interface than RU, despite its larger size. Consequently, RA had slightly higher emulsifying activity than RU at a low protein concentration (0.2 wt%). The higher surface hydrophobicity

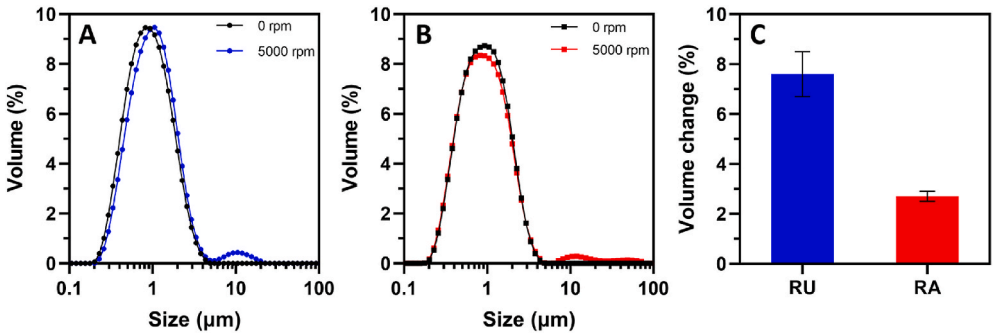

Fig. 11. Droplet size distributions of the emulsions prepared with RU (A) and RA (B) after shear treatment at homogenization speed of 5000 rpm. (C) Volume change (%) of the droplet size of RU- and RA-stabilized emulsions prepared at 1 wt% protein concentration after the shear treatment. **Note**: all measurements were performed in 1 wt% SDS solution.

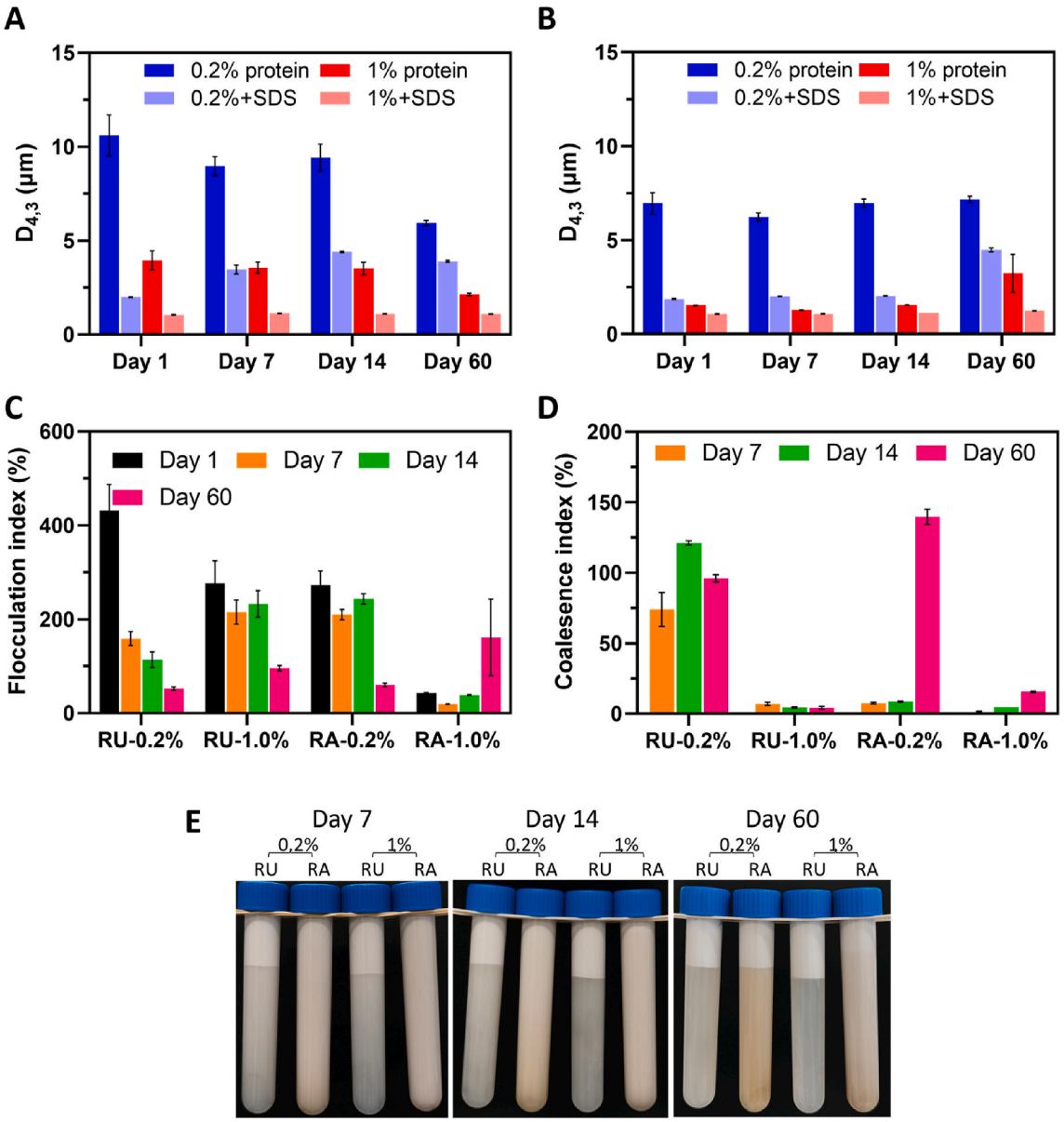

Fig. 12. Volume-weighted-mean droplet size ($D_{4,3}$) of the emulsions stabilized by RU (A) and RA (B) at 0.2 wt% and 1 wt% protein concentration measured in water and in 1 wt% SDS solution during storage for 60 days. Flocculation index (%) (C) and coalescence index (%) (D) of emulsions stabilized by RU and RA at 0.2 wt% and 1 wt% protein concentration during storage. (E) Visual observations of those emulsions during storage.

of RA also enhanced its packing and in-plane interactions at the interface, where the generated interface was stiffer and more resistant to large shear and dilatational deformations compared to the RU-stabilized interface. As a result, the RA-stabilized emulsion was more stable to coalescence in large shear environments, and during storage. Additionally, the increased surface ionic groups of RA from structural reassembly caused higher electrostatic repulsion between emulsion droplets, which pronouncedly increased the stability of emulsions against flocculation and creaming.

Our findings provide new insights into the emulsion stabilization mechanisms of Rubisco from the perspectives of its molecular and oil-water interfacial properties, which are expected to promote the application of Rubisco as a functional ingredient in the food industry. Besides, the exploration of the influence of protein denaturation or structural reassembly on interfacial and emulsifying behavior might help to understand similar effects observed in other denatured proteins such as soy proteins, whey proteins, and ovalbumin (Nir, Feldman, Aserin, & Garti, 1994; Palazolo et al., 2004; Palazolo, Sorgentini, & Wagner, 2005; Voutsinas, Cheung, & Nakai, 1983). These findings demonstrate that structural reassembly might be a useful strategy to improve the behavior of plant proteins in oil-water interface and emulsion stabilization.

The findings from Part I and Part II provide deep insight on the behavior of Rubisco proteins as modulated by protein extraction processes in stabilizing multiphase systems, and could guide future research in plant protein extraction and modification of plant proteins for desired performance in stabilizing foam- and emulsion-based multiphase systems.

CRediT authorship contribution statement

Xingfa Ma: Conceptualization, Investigation, Methodology, Validation, Formal analysis, Visualization, Writing – original draft, Writing – review & editing. **Mehdi Habibi:** Supervision, Writing – review & editing. **Jasper Landman:** Supervision, Writing – review & editing. **Leonard M.C. Sagis:** Supervision, Writing – review & editing. **Penghui Shen:** Conceptualization, Investigation, Methodology, Validation,

Formal analysis, Writing – review & editing.

Data availability

Data will be made available on request.

Declaration of competing interest

The authors declare that they have no known competing financial interests or personal relationships that could have appeared to influence the work reported in this paper.

Acknowledgments

X. Ma acknowledges the funding from China Scholarship Council (CSC NO. 202207940007). P. Shen acknowledges the funding from China Scholarship Council (CSC NO. 202006150032).

Appendix A. Supplementary data

Supplementary data to this article can be found online at https://doi.org/10.1016/j.foodhyd.2024.110820.

References

Aiking, H., & de Boer, J. (2020). The next protein transition. *Trends in Food Science & Technology, 105*, 515–522.
Amine, C., Dreher, J., Helgason, T., & Tadros, T. (2014). Investigation of emulsifying properties and emulsion stability of plant and milk proteins using interfacial tension and interfacial elasticity. *Food Hydrocolloids, 39*, 180–186.
Barbeau, W. E., & Kinsella, J. E. (1988). Ribulose bisphosphate carboxylase/oxygenase (rubisco) from green leaves-potential as a food protein. *Food Reviews International, 4*(1), 93–127.
Bergfreund, J., Bertsch, P., & Fischer, P. (2021a). Adsorption of proteins to fluid interfaces: Role of the hydrophobic subphase. *Journal of Colloid and Interface Science, 584*, 411–417.
Bergfreund, J., Bertsch, P., & Fischer, P. (2021b). Effect of the hydrophobic phase on interfacial phenomena of surfactants, proteins, and particles at fluid interfaces. *Current Opinion in Colloid & Interface Science, 56*, Article 101509.
Bergfreund, J., Diener, M., Geue, T., Nussbaum, N., Kummer, N., Bertsch, P., et al. (2021). Globular protein assembly and network formation at fluid interfaces: Effect of oil. *Soft Matter, 17*(6), 1692–1700.
Cabra, V., Arreguin, R., Vazquez-Duhalt, R., & Farres, A. (2006). Effect of temperature and pH on the secondary structure and processes of oligomerization of 19 kDa alpha-zein. *Biochimica et Biophysica Acta (BBA)-Proteins and Proteomics, 1764*(6), 1110–1118.
Creux, P., Lachaise, J., Graciaa, A., Beattie, J. K., & Djerdjev, A. M. (2009). Strong specific hydroxide ion binding at the pristine oil/water and air/water interfaces. *The Journal of Physical Chemistry B, 113*(43), 14146–14150.
de Groot, A., Yang, J., & Sagis, L. M. (2023). Surface stress decomposition in large amplitude oscillatory interfacial dilatation of complex interfaces. *Journal of Colloid and Interface Science, 638*, 569–581.
Delahaije, R. J. B. M., Kiskini, A., & Wierenga, P. A. (2022). Towards predicting the emulsion properties of plant protein extracts from sugar beet (Beta vulgaris L.) leaf and soybean (Glycine max). *Colloids and Surfaces A: Physicochemical and Engineering Aspects, 646*, Article 128950.
Dickinson, E. (2019). Strategies to control and inhibit the flocculation of protein-stabilized oil-in-water emulsions. *Food Hydrocolloids, 96*, 209–223.
Dumetz, A. C., Chockla, A. M., Kaler, E. W., & Lenhoff, A. M. (2008). Effects of pH on protein–protein interactions and implications for protein phase behavior. *Biochimica et Biophysica Acta (BBA)-Proteins and Proteomics, 1784*(4), 600–610.
El-Mahrab-Robert, M., Rosilio, V., Bolzinger, M.-A., Chaminade, P., & Grossiord, J.-L. (2008). Assessment of oil polarity: Comparison of evaluation methods. *International journal of pharmaceutics, 348*(1–2), 89–94.
Ewoldt, R. H., Hosoi, A., & McKinley, G. H. (2008). New measures for characterizing nonlinear viscoelasticity in large amplitude oscillatory shear. *Journal of Rheology, 52*(6), 1427–1458.
Fan, L., Liu, Y., Huang, S., & Li, J. (2022). Effects of proteins on emulsion stability: The role of proteins at the oil–water interface. *Food Chemistry, 397*, Article 133726.
Geerts, M. E., Nikiforidis, C. V., van der Goot, A. J., & van der Padt, A. (2017). Protein nativity explains emulsifying properties of aqueous extracted protein components from yellow pea. *Food Structure, 14*, 104–111.
Ikenaga, N., & Sagis, L. M. (2024). Interfacial moduli at large strains and stability of emulsions stabilised by plant proteins at high bulk shear rates. *Food Hydrocolloids, 146*, Article 109248.
Kobbi, S., Bougatef, A., Le Flem, G., Balti, R., Mickael, C., Fertin, B., et al. (2017). Purification and recovery of RuBisCO protein from alfalfa green juice: Antioxidative properties of generated protein hydrolysate. *Waste and biomass valorization, 8*, 493–504.
Kornet, C., Venema, P., Nijsse, J., van der Linden, E., van der Goot, A. J., & Meinders, M. (2020). Yellow pea aqueous fractionation increases the specific volume fraction and viscosity of its dispersions. *Food Hydrocolloids, 99*, Article 105332.
Lamsal, B., Koegel, R., & Gunasekaran, S. (2007). Some physicochemical and functional properties of alfalfa soluble leaf proteins. *Lwt-Food Science and Technology, 40*(9), 1520–1526.
Lucassen, J., & Van Den Tempel, M. (1972). Dynamic measurements of dilational properties of a liquid interface. *Chemical Engineering Science, 27*(6), 1283–1291.
Malmsten, M. (1998). Formation of adsorbed protein layers. *Journal of Colloid and Interface Science, 207*(2), 186–199.
Martin, A. H., Castellani, O., de Jong, G. A., Bovetto, L., & Schmitt, C. (2019). Comparison of the functional properties of RuBisCO protein isolate extracted from sugar beet leaves with commercial whey protein and soy protein isolates. *Journal of the Science of Food and Agriculture, 99*(4), 1568–1576.
McClements, D. J. (2004). Protein-stabilized emulsions. *Current Opinion in Colloid & Interface Science, 9*(5), 305–313.
Miriani, M., Corredig, M., Iametti, S., & Bonomi, F. (2011). Denaturation of soy proteins in solution and at the oil–water interface: A fluorescence study. *Food Hydrocolloids, 25*(4), 620–626.
Moghimikheirabadi, A., Fischer, P., Kröger, M., & Sagis, L. M. (2019). Relaxation behavior and nonlinear surface rheology of peo–ppo–peo triblock copolymers at the air–water interface. *Langmuir, 35*(44), 14388–14396.
Mohan, S., & Narsimhan, G. (1997). Coalescence of protein-stabilized emulsions in a high-pressure homogenizer. *Journal of Colloid and Interface Science, 192*(1), 1–15.
Negi, A. S., & Osuji, C. O. (2010). Time-resolved viscoelastic properties during structural arrest and aging of a colloidal glass. *Physical Review E, 82*(3), Article 031404.
Nir, I., Feldman, Y., Aserin, A., & Garti, N. (1994). Surface properties and emulsification behavior of denatured soy proteins. *Journal of Food Science, 59*(3), 606–610.
Ntone, E., Bitter, J. H., & Nikiforidis, C. V. (2020). Not sequentially but simultaneously: Facile extraction of proteins and oleosomes from oilseeds. *Food Hydrocolloids, 102*, Article 105598.
Palazolo, G. G., Sorgentini, D. A., & Wagner, J. R. (2004). Emulsifying properties and surface behavior of native and denatured whey soy proteins in comparison with other proteins. Creaming stability of oil-in-water emulsions. *Journal of the American Oil Chemists' Society, 81*, 625–632.
Palazolo, G. G., Sorgentini, D. A., & Wagner, J. R. (2005). Coalescence and flocculation in o/w emulsions of native and denatured whey soy proteins in comparison with soy protein isolates. *Food Hydrocolloids, 19*(3), 595–604.
Pérez-Vila, S., Fenelon, M. A., O'Mahony, J. A., & Gómez-Mascaraque, L. G. (2024). The emulsifying properties of protein extracts from perennial ryegrass (Lolium perenne L.) depend on the extraction method. *Food Hydrocolloids, 152*, Article 109917.
Perrier-Cornet, J., Marie, P., & Gervais, P. (2005). Comparison of emulsification efficiency of protein-stabilized oil-in-water emulsions using jet, high pressure and colloid mill homogenization. *Journal of Food Engineering, 66*(2), 211–217.
Rawiwan, P., & Quek, S. Y. (2024). Physicochemical and functional attributes of RuBisCo-enriched Brassicaceae leaf protein concentrates. *Food Hydrocolloids*, Article 109887.
Sagis, L. M., & Fischer, P. (2014). Nonlinear rheology of complex fluid–fluid interfaces. *Current Opinion in Colloid & Interface Science, 19*(6), 520–529.
Sanchez de Jimenez, E., Medrano, L., & Martinez-Barajas, E. (1995). Rubisco activase, a possible new member of the molecular chaperone family. *Biochemistry, 34*(9), 2826–2831.
Sengupta, T., & Damodaran, S. (1998). Role of dispersion interactions in the adsorption of proteins at oil– water and air– water interfaces. *Langmuir, 14*(22), 6457–6469.
Shohat, D., Friedman, Y., & Lahini, Y. (2023). Logarithmic aging via instability cascades in disordered systems. *Nature Physics, 19*(12), 1890–1895.
Skipper, J., Hendrickson, R. C., Gulden, P. H., Brichard, V., Van Pel, A., Chen, Y., et al. (1996). An HLA-A2-restricted tyrosinase antigen on melanoma cells results from posttranslational modification and suggests a novel pathway for processing of membrane proteins. *Journal of Experimental Medicine, 183*(2), 527–534.
Tamm, F., & Drusch, S. (2017). Impact of enzymatic hydrolysis on the interfacial rheology of whey protein/pectin interfacial layers at the oil/water-interface. *Food Hydrocolloids, 63*, 8–18.
Tan, Y., Lee, P. W., Martens, T. D., & McClements, D. J. (2022). Comparison of emulsifying properties of plant and animal proteins in oil-in-water emulsions: Whey, soy, and RuBisCo proteins. *Food Biophysics, 17*(3), 409–421.
Tanambell, H., Møller, A. H., Roman, L., Corredig, M., & Dalsgaard, T. K. (2023). Supramolecular structure modification of RuBisCO from alfalfa during removal of chloroplastic materials. *Innovative Food Science & Emerging Technologies, 87*, Article 103408.
Tcholakova, S., Denkov, N. D., Ivanov, I. B., & Campbell, B. (2006). Coalescence stability of emulsions containing globular milk proteins. *Advances in Colloid and Interface Science, 123*, 259–293.
Tziva, M., Negro, S., Kalfagianni, A., & Hekkert, M. (2020). Understanding the protein transition: The rise of plant-based meat substitutes. *Environmental Innovation and Societal Transitions, 35*, 217–231.
Voutsinas, L. P., Cheung, E., & Nakai, S. (1983). Relationships of hydrophobicity to emulsifying properties of heat denatured proteins. *Journal of Food Science, 48*(1), 26–32.
Walstra, P. (1993). Principles of emulsion formation. *Chemical Engineering Science, 48*(2), 333–349.
Wang, W., Li, K., Wang, P., Hao, S., & Gong, J. (2014). Effect of interfacial dilational rheology on the breakage of dispersed droplets in a dilute oil–water emulsion. *Colloids and Surfaces A: Physicochemical and Engineering Aspects, 441*, 43–50.

Wierenga, P. A., Meinders, M. B., Egmond, M. R., Voragen, F. A., & de Jongh, H. H. (2003). Protein exposed hydrophobicity reduces the kinetic barrier for adsorption of ovalbumin to the air− water interface. *Langmuir, 19*(21), 8964–8970.

Winter, H. H., & Mours, M. (1999). Rheology of polymers near liquid-solid transitions. *Neutron spin echo spectroscopy viscoelasticity rheology* (pp. 165–234).

Xia, L.-Y., Jiang, Y.-L., Kong, W.-W., Sun, H., Li, W.-F., Chen, Y., et al. (2020). Molecular basis for the assembly of RuBisCO assisted by the chaperone Raf1. *Nature Plants, 6*(6), 708–717.

Yang, J., & Sagis, L. M. (2021). Interfacial behavior of plant proteins—novel sources and extraction methods. *Current Opinion in Colloid & Interface Science, 56*, Article 101499.

Yang, J., Shen, P., de Groot, A., Mocking-Bode, H. C., Nikiforidis, C. V., & Sagis, L. M. (2024). Oil-water interface and emulsion stabilising properties of rapeseed proteins napin and cruciferin studied by nonlinear surface rheology. *Journal of Colloid and Interface Science, 662*, 192–207.